PLAXIS LIQUEFACTION MODEL
UBC3D-PLM

Alexandros Petalas
Assistant Researcher, PLAXIS B.V

Vahid Galavi
Researcher, PLAXIS B.V

May 30, 2012

Contents

List of Figures

List of Tables

Abstract

In this report the formulation of the UBC3D constitutive model as implemented in PLAXIS is presented. The UBC3D is a 3-D generalized formulation of the original 2-D UBCSAND model introduced by Puebla et al. (1997). The initial 3-D implementation in PLAXIS was presented by Tsegaye (2010). An improved version is developed by the authors and the final model is presented together with a validation in different monotonic and cyclic stress paths. UBC3D-PLM consists a relatively simple but powerful approach in order to model the onset of the liquefaction phenomenon. In Chapter 1 the main features of the UBC3D-PLM are presented. The improvements made by the authors are also highlighted in order to distinguish the changes of the latest version. Briefly, the formulation of the plastic multiplier is corrected and higher accuracy achieved for the monotonic case, a soil densification rule was implemented and a second yield surface introduced in order to ensure a smooth transition into the liquefied state and finally a post liquefaction factor introduced as an input parameter in order to model the post-liquefaction behaviour. The latter should be used for modelling element tests leading to liquefaction of the soil, and extra attention is advised during modelling boundary value problems. In Chapter 2 the validation of the model in monotonic and cyclic stress paths is discussed. Finally, in Chapter 3 the performance of the model in a finite element scheme is investigated and the numerical modelling of a dynamic centrifuge test with PLAXIS 2D Dynamics is presented. The ability of the model to capture the onset of liquefaction is thoroughly discussed. The capabilities and the limitations are highlighted and recommendations for the use of the model are summarized.

Chapter 1

Key Features of UBC3D

The UBC3D-PLM model has been developed by Tsegaye (2010) and implemented as a user-defined model in PLAXIS. It is closely based on the UBCSAND model introduced by Puebla et al. (1997), Beaty and Byrne (1998). The original UBCSAND is a 2-D model developed for prediction of liquefaction in sandy soils. Its formulation is based on classical plasticity theory with a hyperbolic strain hardening rule, based on the Duncan-Chang approach with modifications. The hardening rule relates the mobilized friction angle to the plastic shear strain at a given stress. It contains a 2-D Mohr-Coulomb yield surface and a corresponding non-associated plastic potential function. The flow rule in the model is based on the stress-dilatancy theory developed by Rowe (1962), linearised and simplified according to energy considerations.

The main difference between the UBCSAND model and the UBC3D model is the latter generalized 3-D formulation. The UBC3D model uses the Mohr-Coulomb yield condition in a 3-D principal stress space. Moreover, a modified non-associated plastic potential function based on Drucker-Prager's criterion is used, in order to maintain the assumption of stress-strain coaxiality in the deviatoric plane for a stress path beginning from the isotropic line (Tsegaye, 2010).

Comparing with the previous version of UCB3D implemented in PLAXIS, in the latest version a correction is made in the equation of the plastic multiplier which governs the constitutive relationship between the stresses and strains and higher accuracy is succeeded during monotonic loading. Finally, a soil densification rule is added in order to predict a more realistic evolution of excess pore pressures during cyclic loading. This allows the increase of the volumetric strains with a decreasing rate during shearing. Moreover, the bulk modulus of water is depended on the degree of saturation which is specified via PLAXIS input and therewith this user defined model can be used in the Advanced calculation mode of PLAXIS.

The main characteristics of the model as implemented by (Tsegaye, 2010) and modified by the authors are presented in the following sections.

1.1 Yield Surfaces

The UBC3D-PLM model uses the well known Mohr-Coulomb yield function generalized in 3-D principal stress space. In order to understand how the algorithm deals with the complexity of the 3-D representation of the yield surfaces, the full set of the Mohr-Coulomb yield functions are introduced (pressure is positive, tension is positive):

$$f_{1a} = \frac{1}{2}(\sigma'_2 - \sigma'_3) + \frac{1}{2}(\sigma'_2 + \sigma'_3)\sin\phi' - c'\cos\phi' \tag{1.1}$$

$$f_{1b} = \frac{1}{2}(\sigma'_3 - \sigma'_2) + \frac{1}{2}(\sigma'_3 + \sigma'_2)\sin\phi' - c'\cos\phi' \tag{1.2}$$

$$f_{2a} = \frac{1}{2}(\sigma'_3 - \sigma'_1) + \frac{1}{2}(\sigma'_3 + \sigma'_1)\sin\phi' - c'\cos\phi' \tag{1.3}$$

$$f_{2b} = \frac{1}{2}(\sigma'_1 - \sigma'_3) + \frac{1}{2}(\sigma'_1 + \sigma'_3)\sin\phi' - c'\cos\phi' \tag{1.4}$$

$$f_{3a} = \frac{1}{2}(\sigma'_1 - \sigma'_2) + \frac{1}{2}(\sigma'_1 + \sigma'_2)\sin\phi' - c'\cos\phi' \tag{1.5}$$

$$f_{3b} = \frac{1}{2}(\sigma'_2 - \sigma'_1) + \frac{1}{2}(\sigma'_2 + \sigma'_1)\sin\phi' - c'\cos\phi' \tag{1.6}$$

The six combinations of the principal stresses in the equations define six planes in 3-D principal stress space. These planes defines the Mohr-Coulomb yield surface as presented in Figure 1.1. The projection of the yield surface in the π -plane is presented in Figure 1.2.

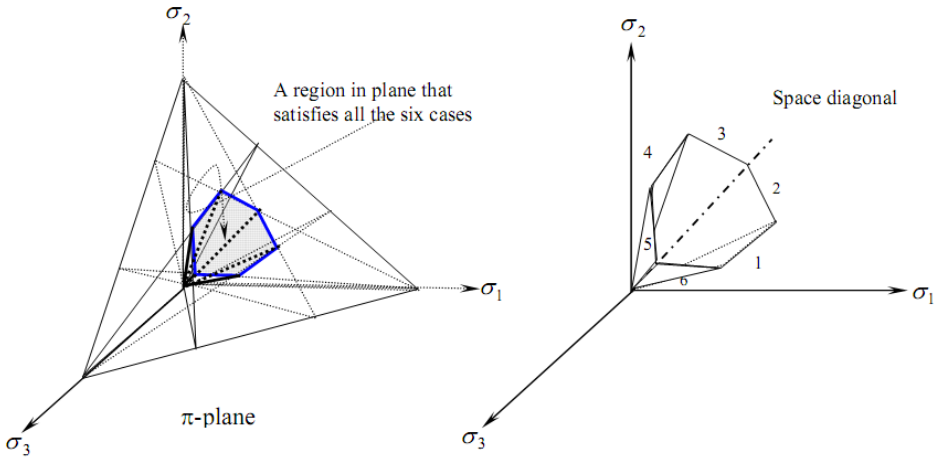

Figure 1.1: The intersection of the six planes and finally the yield surface in 3-D principal stress space. After Tsegaye (2010).

The first step that has to be done by the model is to compute the principal stresses of the stress tensor. This is done after solving the eigenvalue problem. The eigenvalues give the principal stresses and the eigenvectors will be their directions. As far as isotropic behaviour is concerned the directions of the principal stresses are fixed (rotation of the principal stresses is not included in UBC3D-PLM) so the material response is not dependent on the orientation. After the determination of the three principal stresses

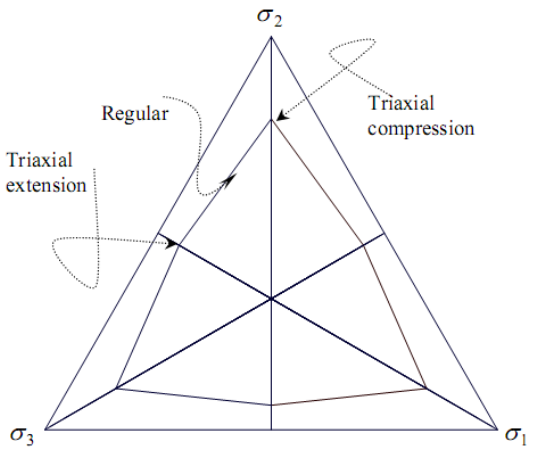

Figure 1.2: Projection of the yield surface in the deviatoric plane. After Tsegaye (2010).

the yield surface has to be defined. Considering any stress path in the generalized 3-D stress space visualized in the deviatoric plane, the yield surface which will be first activated is given by the equation in which the maximum difference between two principal stresses is being used. The critical yield surface in the model is given by Equation 1.7:

$$f_m = \frac{\sigma'_{max} - \sigma'_{min}}{2} - \left(\frac{\sigma'_{max} + \sigma'_{min}}{2} + c' \cot \phi'_p \right) \sin \phi_{mob} \qquad (1.7)$$

The above presented equation is derived by the Mohr-Coulomb failure criterion using the maximum and the minimum principal stress as well as the mobilized friction angle (see Section 1.2). In order to compute Equation 1.7 the principal stresses are sorted as follows:

$$-\sigma_1 \geq -\sigma_2 \geq -\sigma_3 \qquad (1.8)$$

After the sorting and the development of the yield surface, three possible stress paths can be produced by the model, in one of the six parts of the π-plane; triaxial compression, triaxial extension and regular stress path, as depicted in Figure 1.2.

Referred to as the apex term, $c \cot \phi_p$ defines the point where the yield surface intersects the mean effective stress axis (p) (see Figure 1.3). Usually, in granular soils, the cohesion is zero, so the intersection would be located at the origin of the coordinate system (0,0).

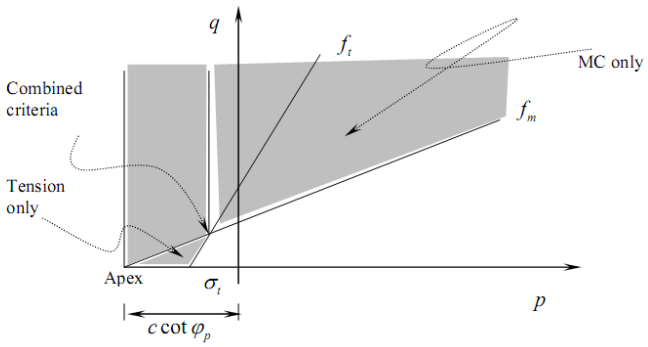

Figure 1.3: Systematization of the yield surfaces in p-q stress space. After Tsegaye (2010).

When the stress state is inside the space defined by the yield surfaces elastic behaviour is assumed. However, once the stress path touches the yield surface plasticity starts to occur. After the reformulation made by the authors the latest version of the UBC3D-PLM has two yield surfaces in order to distinguish between the primary and the secondary loading and to ensure a smooth transition to the liquefied state. This mechanism is better explained in Section 1.5. The elasto-plastic behaviour of the model will be analytically presented in the next paragraph.

1.2 Elasto-plastic Behaviour and Hardening Rule

The elastic behaviour which occurs within the yield surface is governed by a non-linear rule. Two parameters control this non-linear behaviour; the elastic bulk modulus K and the elastic shear modulus G. These two moduli are stress dependent and the relationships are given in the following equations:

$$K = K_B^e P_A \left(\frac{p}{P_{ref}} \right)^{me} \tag{1.9}$$

$$G = K_G^e P_A \left(\frac{p}{P_{ref}} \right)^{ne} \tag{1.10}$$

where K_B^e and K_G^e are the bulk and the shear modulus respectively, at a reference stress level. The factors ne and me are parameters define the rate of stress dependency of stiffness. In the literature, the reference stress level (p_{ref}) is commonly taken as the atmospheric pressure (P_A=100 kPa). Pure elastic behaviour is predicted by the model during the unloading process.

Once the stress state reaches the yield surface, plastic behaviour is predicted as long as the stress point is not going immediately back into the elastic zone. More specifically, plastic hardening based on the principal of strain hardening is used in the model. The hardening rule governs the amount of plastic strain (irrecoverable deformation) as a result of mobilization of the shear strength ($\sin\phi_{mob}$). The mobilized friction angle derived from the Mohr-Coulomb yield criterion (1.7) is given as:

$$\sin\phi_{mob} = \frac{\sigma_1' - \sigma_3'}{\sigma_1' + \sigma_3'} = \frac{t_{mob}}{s'} \tag{1.11}$$

where t_{mob} is the mobilized shear stress and s is the mean effective stress (s).

The hyperbolic hardening rule (Beaty and Byrne, 1998) is presented schematically in Figure 1.4. It relates the increment of the sine of the mobilized friction angle to the plastic shear strain increment as follows (Puebla et al., 1997):

$$\delta\gamma^p = \left(\frac{1}{G^\star} \right) \delta \sin\phi_{mob} \tag{1.12}$$

$$G^\star = k_G^p \left(\frac{p'}{P_A} \right)^{np} \left\{ 1 - \left(\frac{\sin\phi_{mob}}{\sin\phi_{peak}} \right) R_F \right\}^2 \tag{1.13}$$

where k_G^p is the plastic shear modulus number; np is the plastic shear modulus exponent; ϕ_{mob} is the mobilized friction angle, which is defined by the stress ratio; ϕ_{peak} is the peak friction angle; and R_f is the failure ratio n_f/n_{ult}, ranging from 0.5 to 1.0, where n_f is the stress ratio at failure and n_{ult} is the asymptotic stress ratio from the best fit hyperbola.

The hardening rule as reformulated by Tsegaye (2010) in UBC3D-PLM model is given as:

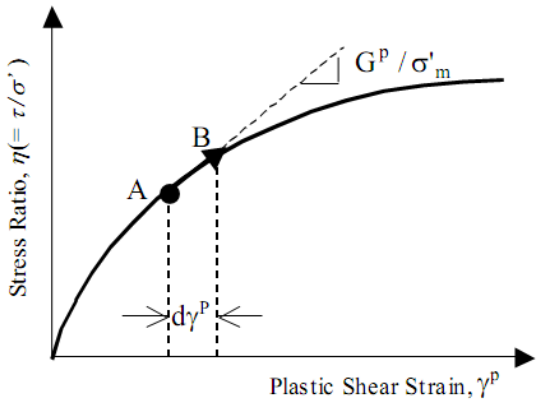

Figure 1.4: The original UBCSAND's Hardening Rule. From Beaty and Byrne (1998)

$$d\sin\phi_{mob} = 1.5K_G^p\left(\frac{p}{p_A}\right)^{np}\frac{p_A}{p_m}\left(1-\frac{\sin\phi_{mob}}{sin\phi_{peak}}R_f\right)^2 d\lambda \tag{1.14}$$

where $d\lambda$ is the plastic strain increment multiplier.

1.3 Plastic Potential Function

The plastic potential function specifies the direction of the plastic strain. A non-associated flow rule based on the Drucker-Prager plastic potential function is used in the UBC3D-PLM (Tsegaye, 2010).

The plastic potential function is formulated as:

$$g = q - a\left(p' + c\cot\phi_p\right) \tag{1.15}$$

$$a = \frac{\sqrt{3}\sin\psi_{mob}}{\cos\theta + \frac{\sin\theta\sin\psi}{\sqrt{3}}} \tag{1.16}$$

where θ is taken 30° to fit the Drucker-Prager surface in the compression point.

1.4 Flow Rule

In the UBC3D-PLM model the flow rule of the original UBCSAND model is used, which is derived from energy considerations by Puebla et al. (1997). The flow rule used in UBCSAND is based on three observations: 1. there is a unique stress ratio, defined by the constant volume friction angle ϕ_{cv}, for which plastic shear strains do not cause plastic volumetric strains; 2. stress ratios which lie below $\sin\phi_{cv}$ exhibit contractive behaviour, while stress ratios above $\sin\phi_{cv}$ lead to a dilative response; and, 3. the amount of contraction or dilation depends on the difference between the current stress ratio and the stress ratio at $\sin\phi_{cv}$.

The relationship is given as follows:

$$d\epsilon_v^p = \sin\psi_m d\gamma^p \tag{1.17}$$

$$\sin\psi_m = \sin\phi_m - \sin\phi_{cv} \tag{1.18}$$

where, $d\epsilon_v^p$ is the plastic volumetric strain increment and ϕ_{cv} is the constant volume friction angle. A graphical representation of the flow rule is give in Figure 1.5.

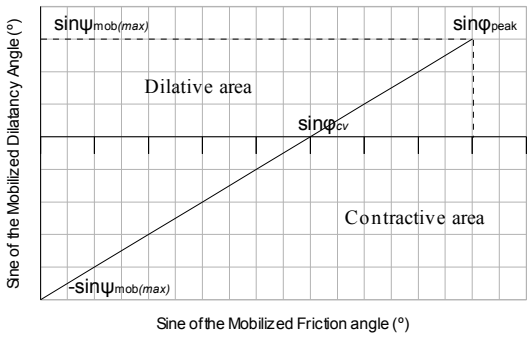

Figure 1.5: Graphical representation of the modified Rowe's flow rule as used in UBC3D-PLM.

1.5 Cyclic Mobility and Stress Reversal

Based on the mobilized friction angle an unloading-reloading criterion is defined in the model as follows:

$$\sin\phi_m^e < \sin\phi_m^0 \textit{(Unloading; elastic behaviour.)} \tag{1.19}$$

$$\sin\phi_m^e > \sin\phi_m^0 \textit{(Loading or reloading; plastic behaviour.)} \tag{1.20}$$

The previous mobilized friction angle ($\sin\phi_m^o$) is memorized from the previous calculation step, while the current one ($\sin\phi_m^e$) is calculated based on the current stresses. During loading, the friction angle is mobilized, and hardening plasticity occurs. During unloading, pure elastic behaviour is predicted until the stress point reaches the p' axis.

A soil densification rule was introduced in the latest verion of the UBC3D-PLM in order to have higher accuracy in the predicted evolution of the excess pore pressures. A secondary yield surface was introduced in the model for

the secondary loading in order to ensure a smooth transition into the liquefied state of the soil. This enables the distinction between primary and secondary loading.

The secondary yield surface generates less plastic strains compared to the primary yield surface. An isotropic hardening rule is used for the primary yield surface, while a simplified kimematic hardening rule is used for the secondary surface. The plastic shear modulus K_G^p during primary loading is identical with the one entered as input parameter by the user and is used in the hardening rule governing the hardening of the primary yield surface. The plastic shear modulus K_G^p during the secondary loading is formulated as a function of the number of cycles followed during the loading process in order to capture the effect of soil densification during drained shearing reported by many researchers in the literature (Martin et al., 1975). A simple rule which defines the counting process of cycles is used. This leads to an increase of the excess pore pressure during uncdrained cyclic loading with a decreasing rate until the liquefied state is approached.

The densification rule is fully valid for symmetric loading cycles, for the case that shearing starts from the isotropic stress state. In a $p' - q$ stress space when the mobilized friction angle is very small a half cycle is counted. The drained plastic shear modulus (K_G^p) becomes stiffer after the first full cycle using Equation 1.24. This densification rule has been calibrated against experimental data for the behaviour of sands under cyclic simple shearing.

$$K_G^p = K_G^p * \left(4 + \frac{n_{cross}}{2}\right) * hard * fac_{hard} \tag{1.21}$$

where n_{cross} is the number of half cycles generated from the beginning of the test, $hard$ is a factor which is correcting the densification rule for loose soils and fac_{hard} is a multiplier which is a user input parameter to adjust the densification rule.

A correction is made in the densification rule for loose sands ($5 \leq N1_{60} \leq 9$) according to the experimental observations and following the formulation

of the UBCSAND proposed by Beaty and Byrne (2011) and reported by Naesgaard (2011). The correction rule is as follows:

$$hard = min(1, max(0.5, 0.1N1_{60}) \tag{1.22}$$

The plastic shear modulus is limited according to the maximum corrected SPT value ($N1_{60}$) of corresponding dense soils (Equation 1.23). The maximum $N1_{60}$ for a very dense soil is defined as 60.

$$K^p_{G,max} = K^e_G * (maxN1^2_{60,max})0.003 + 100 \tag{1.23}$$

The new yield surfaces are schematically presented in Figure 1.6. In Case *a*, primary loading occurs during the first half cycle in an arbitrary simple shear test starting from the p' axis. The initial input parameter for the plastic shear modulus K^p_G is used and both yield surfaces expand until the maximum stress state.

In Case *b*, elastic unloading occurs and the secondary yield surface shrinks until it reaches the isotropic axis where $\sin\phi_{mob}$ is very small. A half cycle is counted. Since an isotropic hardening rule is used for the primary yield surface, it remains at the maximum stress state reached since the beginning of the test.

In Case *c* secondary loading occurs but with an identical plastic shear modulus as used in primary loading followed by elastic unloading. A full cycle is counted. After the full cycle the densification rule is activated.

In Case *d* secondary loading occurs with a plastic shear modulus 4.5 times stiffer than used in primary loading. The secondary yield surface expands until it reaches the maximum stress state of the primary yield surface. Then primary loading is predicted again until the new maximum stress state.

Finally, in case *e*, when the primary yield surface touches the peak stress state (governed by the peak friction angle) the secondary yield surface is deactivated. After the deactivation of the secondary yield surface the primary

loading surface is used again. A new input parameter is defined at this stage in order to include the post-liquefaction behaviour of the soil. If a non zero multiplier fac_{post} is specified, from that stage in the primary yield surface a modified plastic shear modulus will be used based on the following equation:

$$K_G^p = K_G^p * fac_{post} \tag{1.24}$$

If the fac_{post} parameter is less than one the post-liquefaction behaviour of the soil is approximated. This process is consistent with experimental observation and in reality the plastic shear modulus is much lower when the soils passes in the liquefied state. If the factor equals one then a plastic modulus identical to that used in primary loading is taken. Both possibilities are depicted in case e. The influence and the validation of the post liquefaction factor is still under investigation and research and it is recommended to use this factor only in element tests and not in boundary value problems.

1.6 Undrained behaviour in UBC3D-PLM

The undrained behaviour of the soil is treated implicitly by the UBC3D-PLM constitutive model. Therefore, the increment of the pore water pressure is computed at each step of the analysis. Considering a saturated soil specimen, the increments in total stress during loading is given by the following equation:

$$dp = K_u d\epsilon_v \tag{1.25}$$

where K_u is the bulk modulus of the undrained soil and $d\epsilon_v$ the volumetric strain of the soil as a whole.

The effective stress increment can be computed as follows:

$$dp' = K' d\epsilon_v \tag{1.26}$$

where K' is the bulk modulus of the soil skeleton and $d\epsilon_v$ its volumetric strain.

The increments of the pore water pressure is computed with the following equation:

$$dp_w = \frac{K_w}{n} d\epsilon_v \tag{1.27}$$

where K_w is the bulk modulus of the water, n is the soil porosity and $d\epsilon_v$ is the volumetric strain of the fluid.

The relationship between the total stresses, the effective stresses and the pore pressure is assumed according to Terzaghi's theory (Equation 1.28). Moreover, the volumetric compatibility under undrained conditions requires that the equivalent fluid volumetric strain must be equal to the volumetric strain of the soil skeleton. Equation 1.29 is finally derived.

$$dp = dp' + dp_w \tag{1.28}$$

$$\frac{K_w}{n} = (K_u - K') \tag{1.29}$$

Once K_w is determined, then the excess pore pressures can be computed in each increment using Equation 1.27. The Poisson's ratio for undrained condition is set as $\nu = 0.495$ implicitly by the model. This value is close to the upper limit (of 0.5) as water is almost incompressible. Using a value of 0.5 is to be avoided as this is known to cause numerical instabilities. Based on this Poisson's ratio the bulk modulus of the undrained soil is computed as follows:

$$K_u = \frac{2G^e(1 + \nu_u)}{3(1 - 2\nu_u)} \tag{1.30}$$

where G^e is the elastic shear modulus.

The drained bulk modulus of the soil skeleton K' is computed in the same way using the drained Poisson's ratio which is based on the stress dependent stress moduli (Equation 1.31).

$$\nu' = \frac{3K^e - 2G^e}{6K^e + 2G^e} \tag{1.31}$$

In the latest version of the UBC3D the bulk modulus of water is dependent on the degree of saturation of the soil. This enables the prediction of the pore pressure evolution in unsaturated soils. The bulk modulus of the unsaturated water is defined as follows:

$$K_w unsat = \frac{K_w^{Sat} K_{air}}{SK_{air} + (1 - S)K_w^{Sat}} \tag{1.32}$$

where K_w^{Sat} is the bulk modulus of the saturated water and K_{air} is the bulk modulus of air which equals 1 kPa in this implementation having the minimum value. This enables to avoid the generation of pore pressures during modelling a dry sand. under atmospheric pressure. Finally, S is the degree of saturation in the soil.

In this chapter the formulation of the UBC3D-PLM model has been thoroughly discussed. The following chapter presents the validation of the model under triaxial conditions, in order to investigate how well characteristic soil behaviour is captured.

1.7 Parameter selection, summary of the UBC3D input parameters and state variables

In Table 1.7 the input parameters for the UBC3D-PLM model are presented. The main extracting method of the parameters is by fit the experimental curves from element tests. It is crucial to pick the proper element test depends on the stress path which will be the critical during the modelling process. Usually, in earthquake engineering when the onset of liquefaction

is the modelling target a drained cyclic direct simple shear test (DSS) is the proper test in order to be able to extract all the parameters for the UBC3D model.

However, in many cases only data from drained triaxial tests are available (CD TxC). As the triaxial test does not involve principal stress rotation, the test data cannot in principal reflect soil response under principal stress rotation (Vaid et al., 1995). Puebla et al. (1997) proposed a set of equations to be used in the original UBCSAND in order to include the effect of the rotation of principal stresses in terms of stiffness. The equations proposed are derived by experimental observations and fit to the formulation of the UBC3D-PLM constitutive model also. They are derived as follows:

$$For, \quad 0^o \leq a_\sigma \leq 45^o, \quad then \quad K_G^p = (K_G^p)_0\{F - (F-1)\cos 2a\} \tag{1.33}$$

$$For, \quad 45^o \leq a_\sigma \leq 90^o, \quad then \quad K_G^p = (K_G^p)_0 F \tag{1.34}$$

Where:

- and a_σ is the angle between the major principal stress direction and the vertical axis.
- $(K_G^p)_0$ is the plastic modulus number corresponding to $a_\sigma = 0°$ (vertical compression);
- F is the factor of anisotropic plastic response which is less than unity (proposed value 0.317);

With the use of the proposed equations the plastic shear modulus (K_G^p which is proper for modelling the direct simple shear stress path ($a_\sigma = 45°$) is possible if the one suits for triaxial compression is known. Even though with this specific formulation the effect of principal stress rotation in terms of stiffness during plastic hardening can be modelled, the limitations of

modelling the inherent and induced anisotropy in the framework of classical plasticity still arise. The proposed equations were derived only in order to overcome the limitation of using parameters generated from triaxial compression tests which is a common procedure in engineering practice.

Finally, some equations for the derivation of the parameters are published by Beaty and Byrne (2011) for the initial calibration of the model as generic input parameters. These correlations are based on SPT values after calibration of the UBCSAND with proposed analytical solutions and experimental results. The UBC3D-PLM shows a good agreement with the UBCSAND in this stage of development. However, if only the $N1_{60}$ is used for the preliminary parameter selection, the model has to be calibrated with experimental data.

The input parameters of the UBC3D are summarized bellow:

- ϕ_{cv} is the constant volume friction angle;
- ϕ_p is the peak friction angle;
- c is the cohesion of the soil;
- K_B^e is the elastic bulk modulus of the soil in a reference level of 100 kPa. It can be derived from a drained triaxial test with a confining pressure of 100 kPa. When data from a triaxial test with a different confining pressure are available, it can be corrected using Equation 1.9;
- K_G^e is the elastic shear modulus of the soil in a reference level of 100 kPa. It can be related with the K_B^e using the Poison ratio as shown in Equation 1.35;
- K_G^p is the plastic shear modulus and has to be extracted after curve fit;
- me is the elastic bulk modulus index and has a default value of 0.5;

- ne is the elastic shear modulus index and has a default value of 0.5;
- np is the plastic shear modulus index and has a default value of 0.5;
- R_f is the failure ratio n_f/n_{ult} like in Duncan-Chang mode (0.9);
- P_A is the atmospheric pressure;
- fac_{hard} is the densification factor. It is a multiplier that controls the scaling of the plastic shear modulus during secondary loading. Above 1 the K_G^p becomes higher and the behaviour stiffer and bellow 1 the K_G^p becomes lower and the behaviour softer;
- $N1_{60}$ is the corrected SPT value of the soil. If this is not known an approximation with relative density can be made as shown in Equation 1.36;
- fac_{post} is a factor can be used to soft the behaviour of the soil during the post liquefaction behaviour. It is not recommended to use it in boundary value problems but only in element tests. If is not used a value of 1 or 0 can be entered;

$$\frac{K_B^e}{K_G^e} = \frac{2(1+\nu')}{3(1-2\nu')} \tag{1.35}$$

$$N1_{60} \approx \frac{RD^2}{15^2} \tag{1.36}$$

$$PPR = \frac{p_i' - p_c'}{p_i} \tag{1.37}$$

where p_i' is the initial effective mean stress and p_c' is the current effective mean stress. When PPR equals 1 then the soil is in a liquefied state. The PPR state variable can show the current status during the calculation

Table 1.1: Input Parameters for the UBC3D.

Name	Symbol	Unit	Method	Default
Constant volume friction angle	ϕ_{cv}	(°)	CD TxC or DSS	-
Peak friction angle	ϕ_p	(°)	CD TxC or DSS	-
Cohesion	c	kPa	CD TxC or DSS	0
Elastic Shear Modulus	K_G^e	-	Curve Fit	-
Elastic Plastic Modulus	K_G^p	-	Curve Fit	-
Elastic Bulk Modulus	K_B^e	-	Curve Fit	-
Elastic Shear Modulus Index	ne	-	Curve Fit	0.5
Elastic Bulk Modulus Index	me	-	Curve Fit	0.5
Plastic Shear Modulus Index	np	-	Curve Fit	0.5
Failure Ratio	R_f	-	Curve Fit	0.9
Atmospheric Pressure	P_A	kPa	Standard Value	100
Tension Cut-off	σ_t	kPa	-	0
Densification Factor	fac_{hard}	-	Curve Fitting	1
SPT value	$N1_{60}$	-	In-Situ Testing	-
Post Liquefaction Factor	fac_{post}	-	Curve Fitting	0

Table 1.2: State variables of the UBC3D.

Name	Symbol	Explanation
Mobilized Friction Angle	$sinphi\_mob$	Equation 1.11
Maximum Mobilized Friction Angle	max$sinphi_mob$	-
Internal Variable	$etham\_r$	Equals with the $sinphi\_mob$
Number of Cross Over	$xCross$	Number of half cycles
Internal Variable	$dsinphi\_mob$	evolution of $sinphi\_mob$
Confining Factor	$facConf$	Always 1 in this version
Internal Variavle	$PhiPReached$	It is 1 when the ϕ_{peak} is reached
Internal Variable	r_u	Equation 1.38
Initial mean stress	$p0$	In the beginning of the dynamic phase
Pore pressure ratio	PPR	Equation 1.37
Initial vertical stress	$SigV0$	-
Maximum Pore pressure ratio	$PPRMax$	-
Maximum r_u	r_uMax	-

whereas the $PPRMAX$ can reveal if the soil had been in the liquefied state even once during the test. The state variable r_u gives similar information as PPR but instead of the effective mean stress the vertical effective stress is used in the equation as shown in Equation 1.38.

$$r_u = \frac{\sigma'_{vertical,i} - \sigma'_{vertical,c}}{\sigma'_{vertical,i}} \tag{1.38}$$

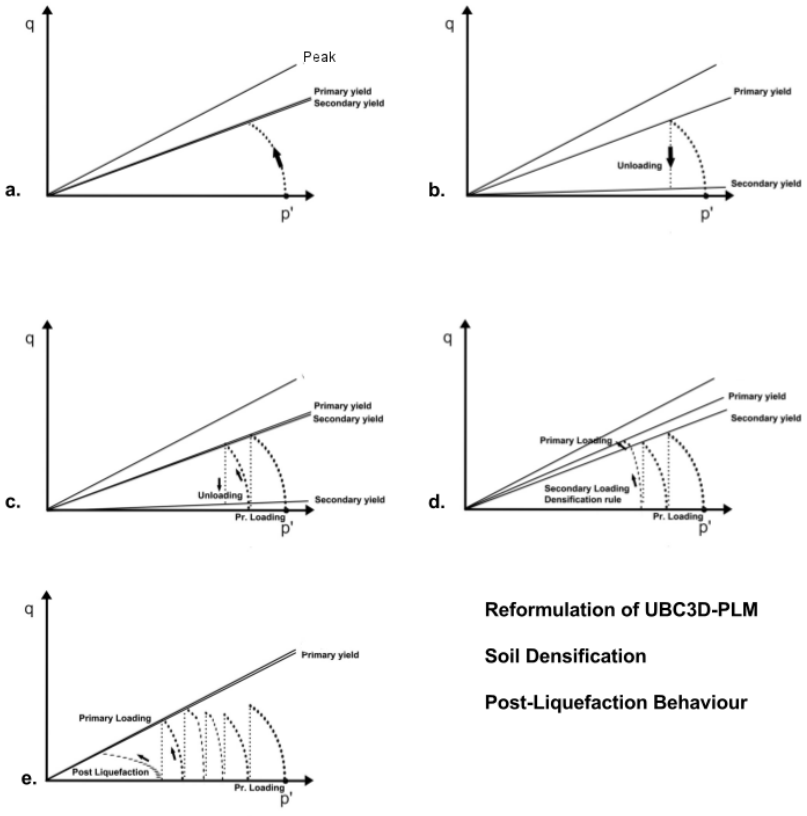

Figure 1.6: Introduction of two yield syrfaces in order to include soil densification, smooth transition in liquefaction state and post-liquefaction behaviour.

Chapter 2

Validation of the UBC3D in various stress paths

2.1 Validation of the reformulated UBC3D-PLM in monotonic loading

In this section the validation of the UBC3D-PLM under monotonic loading is presented. The numerical modelling of a monotonic triaxial compression (TxC) and a monotonic simple shear test (DSS) are shown and compared with experimental data, as well as with the original UBCSAND as published by Beaty and Byrne (1998).

The parameters used in the tests are extracted from a drained triaxial test. The plastic anisotropic factor is used to modify the plastic shear modulus used in UBC3D-PLM in PLAXIS as proposed by Puebla et al. (1997). The parameters are summarized in Table 2.1.

$\phi_p(^\circ)$	$\phi_c(^\circ)$	K_B^e	K_G^e	$K_G^p(TxC)$	$K_G^p(DSS)$	R_f	F
33.7	33	300	300	310	98.3	0.95	0.317

Table 2.1: Model parameters used to simulate undrained behaviour of loose Syncrude sand (Puebla et al., 1997). The stiffness parameters determined in reference stress level of 100 kPa and are unitless. me=ne=0.5, np=0.67.

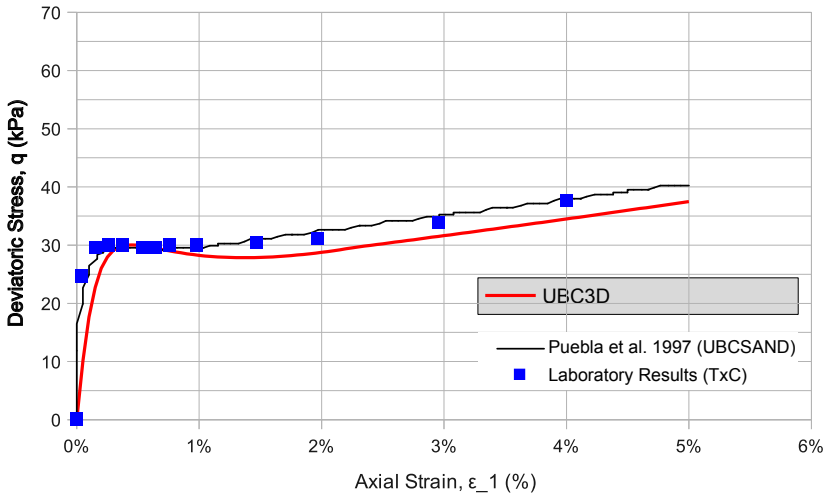

Figure 2.1: Validation of the UBC3D-PLM under monotonic triaxial compression. Undrained behaviour of loose Syncrude sand. Isotropic consolidation with $p' = 100$. The data from the numerical calculation and the experimental result are published by Beaty and Byrne (1998).

In Figure 2.1 the results for the numerical modelling of a triaxial compression test are presented. It can be seen that the reproduced soil behaviour from the UBC3D-PLM high accuracy and is in close agreement with both the experimental data and the results from the original UBCSAND. In Figure 2.2 the results for the numerical calculation of a monotonic direct simple shear test are presented. The UBC3D-PLM model is in good agreement both with the experimental data and the results from the original UBCSAND for this stress path. The model shows a stiffer undrained hardening behaviour in small strain but this can be improved after a better calibration of the input parameters specifically for the proposed model. In this test the parameters are calibrated based on the original UBCSAND.

It is concluded that the UBC3D can model the undrained behaviour of loose sand with high accuracy.

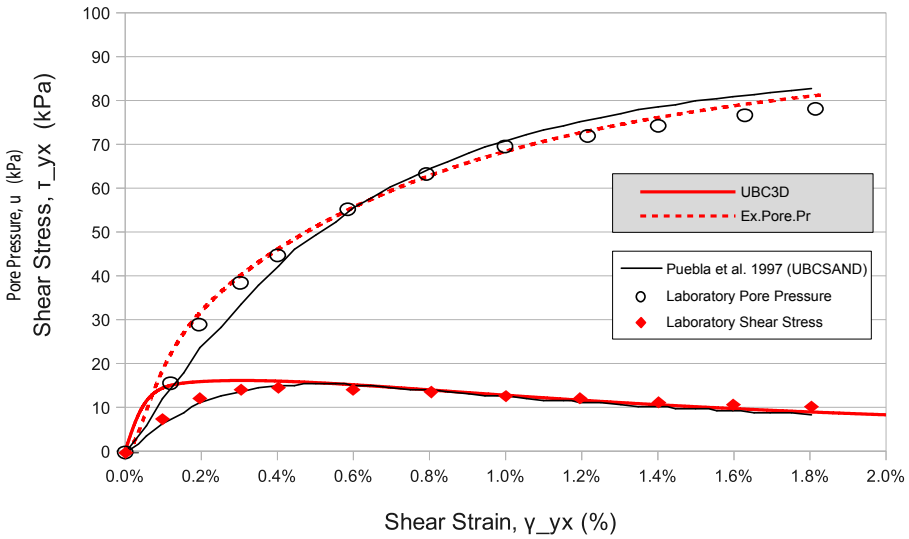

Figure 2.2: Validation of the UBC3D-PLM under monotonic direct simple shear. Undrained behaviour of loose Syncrude sand. Vertical applied stress 100 kPa. The data from the numerical calculation and the experimental result are published by Beaty and Byrne (1998).

2.2 Validation of the reformulated UBC3D-PLM in cyclic loading

In this section the UBC3D-PLM model is validated in undrained cyclic simple shearing. The numerical results are compared with experimental data. The data of the experiments are extracted from the project entitled "Earthquake Induced Damage Mitigation from Soil Liquefaction" which took place in the University of British Columbia "UBC-Liquefaction". An extensive presentation of the experimental results is published in the literature from Sriskandakumar (2004).

Three undrained cyclic direct simple shear experiments on Fraser sand are initially simulated. The relative density (RD) of the sand equals 40% and the applied vertical stress equals 100 kPa. For each test a different cyclic

stress ratio (CSR) is applied. The numerical simulations are carried out at a single stress point using UBC3D-PLM in PLAXIS Soil Test facility. The initial stress conditions for the stress point are described in Table 2.2. The parameters are summarized in Table 2.3. Isotropic consolidation is studied in the first calculation and the influence of a lower K_0 is presented later.

Test	$\sigma^0_{yy}(kPa)$	τ^0_{yx}	$\Delta\epsilon_{xx}$	$\Delta\sigma_{yy}$	$\Delta\epsilon_{zz}$	$\Delta\tau_{yx}(kPa)$	K_0	CSR
1	-100	0	0	0	0	8	1	0.08
2	-100	0	0	0	0	10	1	0.1
3	-100	0	0	0	0	12	1	0.12

Table 2.2: **Boundary values for simulating a cyclic simple shear test in a single stress point. Compression negative. Stresses in kPa.**

$\phi_p(^\circ)$	$\phi_c(^\circ)$	K^e_B	K^e_G	K^p_G	me	ne	np	R_f
33.8	33	607	867	266	0.5	0.5	0.4	0.81

Table 2.3: **Input parameters for modelling the undrained cyclic behaviour of loose Fraser sand. For UBC3D-PLMU7,** $N1_{60} = 8$ **and** $fac_{post} = 0.6$**.**

In Figure 2.3 both the predicted and the experimental stress paths for Test 1 ($CSR = 0.08$) are presented. The UBC3D-PLM model gives adequate accuracy for the specific stress path. The primary loading and the secondary loading with densification can be distinguished, as well as the transition to the liquefied state. Moreover, the post-liquefaction factor which was introduced ensures a much more realistic behaviour of the soil after liquefaction.

Figure 2.4 presents the evolution of the excess pore pressure during the experiment. The UBC3D-PLM predicts the liquefaction of the soil after 15 cycles, whereas in the experiment it occurs after 17 cycles.

In Figure 2.5 the shear stress-strain relationship for the same sand is presented. It can be seen that the use of the post-liquefaction factor fac_{post} gives an accurate approximation of the maximum shear strain during the

first cycle of post-liquefaction behaviour. The maximum shear strain predicted by the model is up to 4.5% and is in a good agreement with the first cycle during the post-liquefaction behaviour.

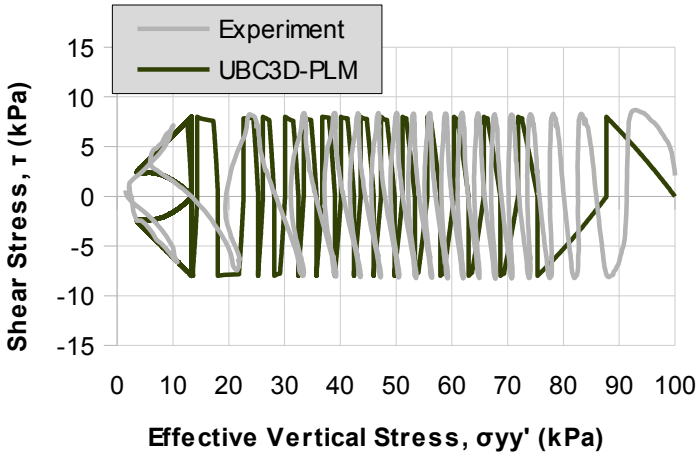

Figure 2.3: Validation of UBC3D-PLM in cyclic loading. Undrained behaviour of Fraser sand ($RD = 40\%$) under cyclic simple shear. Stress path in Test 1 with $CSR = 0.08$.

Figure 2.6 presents the evolution of the excess pore pressure in the experiment and as predicted by UBC3D-PLM for Test 2 ($CSR = 0.1$). The model shows a close agreement with the experimental results. Figure 2.7 presents the evolution of the excess pore pressure both in the experiment and as predicted by the model for Test 3 ($CSR = 0.12$). It can be seen that during the experimental test the soil liquefies after the first 2 cycles and the loading conditions are identical with primary loading, whereas in the numerical calculation (UBC3D-PLM) densification is activated which makes the curve softer. The soil is finally liquefied after 3, which is still a very good approximation of the reality.

The limitation of UBCSAND to predict accurately the soil behaviour during simple shearing in samples which are anisotropically consolidated was

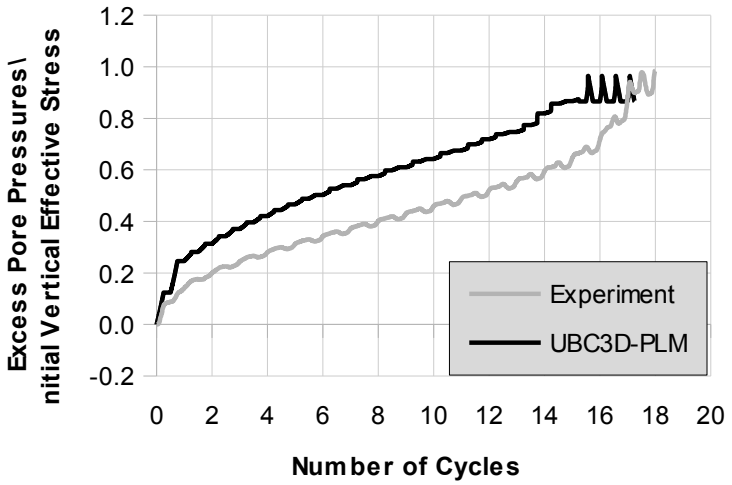

Figure 2.4: Validation of UBC3D-PLM in cyclic loading. Evolution of the excess pore pressure in Test 1. Fraser sand with $RD = 40\%$. $CSR = 0.08$.

investigated in the literature by Park and Byrne (2004). This limitation is also presented in this version. In Figure 2.8 the accumulated pore pressure from the numerical predictions for Test 1 ($CSR = 0.08$) when K_0 equals 0.5 is presented. The accuracy of the model is lower in this case, but the results are accepted for modelling such a complicated phenomenon.

In Figure 2.9 and 2.10 the numerical calculations for Test 2 ($CSR = 0.1$) and 3 ($CSR = 0.12$) are presented respectively. The model gives higher accuracy for these CSR compared to Test 1. A final observation in the predicted soil behaviour after anisotropic consolidation which explains the final results, is that in the UBC3D-PLM when the stress path starts from the K_0 line and reaches the isotropic axis during loading, the primary yield surface with the initial value of plastic shear modulus is activated and the model predicts a rapid increase to the excess pore pressure. The predicted soil behaviour with the UBC3D-PLM during loading when the stress path starts from a K_0 different than 1 will be further improved in the next version.

Finally, in Figure 2.11 a drained strain controlled cyclic direct simple

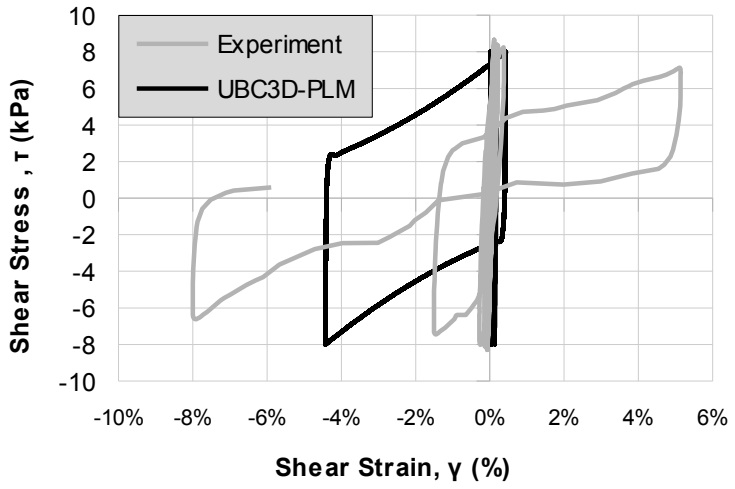

Figure 2.5: Validation of UBC3D-PLM in cyclic loading. Stress-strain relationship of Fraser sand with $RD = 40\%$ in Test 1. $CSR = 0.08$.

shear test on the same soil is modelled with constant applied strain up to 3%. The first cycle is highlighted. It can be concluded that the constitutive model over-produces hysteretic damping in the system because of the linear elastic unloading rule with constant shear modulus equals G_{max}. This leads to bigger area of the hysteretic loop, which equals with the amount of predicted damping. This fact is well documented in the literature also for the UBCSAND model (Beaty and Byrne, 2011) and is an intrinsic characteristic of the model.

In the final chapter the validation of the reformulated version in a finite element scheme is presented. This gives the opportunity to investigate the limitations of the reformulated version during non-symmetric cycles, under different stress paths during the test and finally to have a clearer opinion on the influence of the K_0 value.

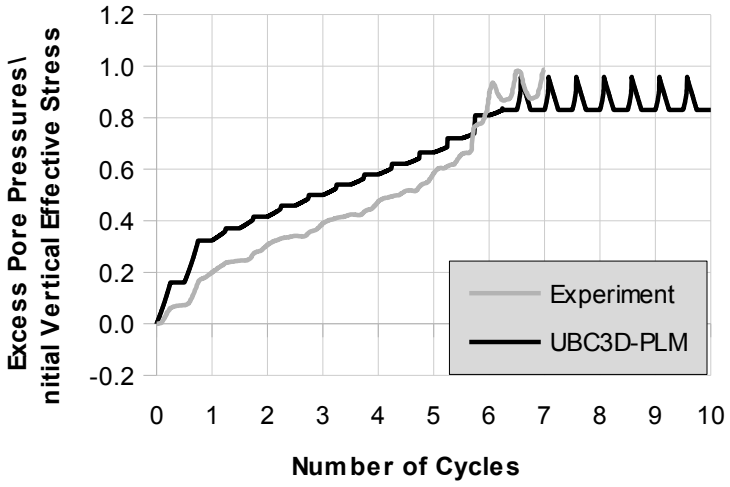

Figure 2.6: Validation of UBC3D-PLM for cyclic loading. Evolution of the excess pore pressure in Test 2. Fraser sand with $RD = 40\%$. $CSR = 0.1$.).

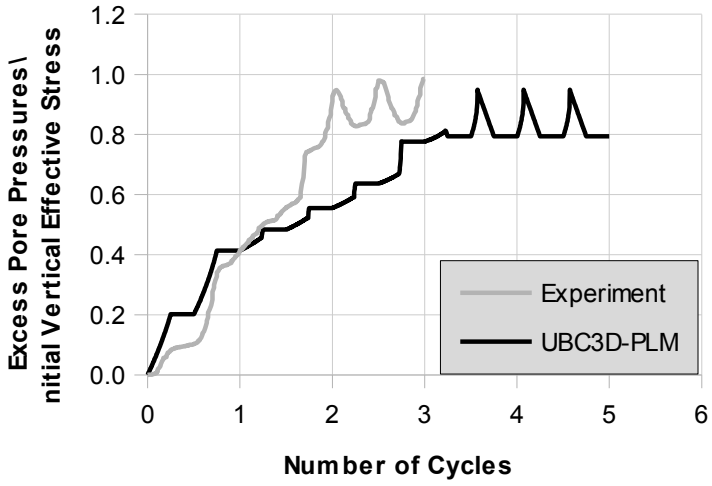

Figure 2.7: Validation of UBC3D-PLM for cyclic loading. Evolution of the excess pore pressure in Test 3. Fraser sand with $RD = 40\%$. $CSR = 0.12$.

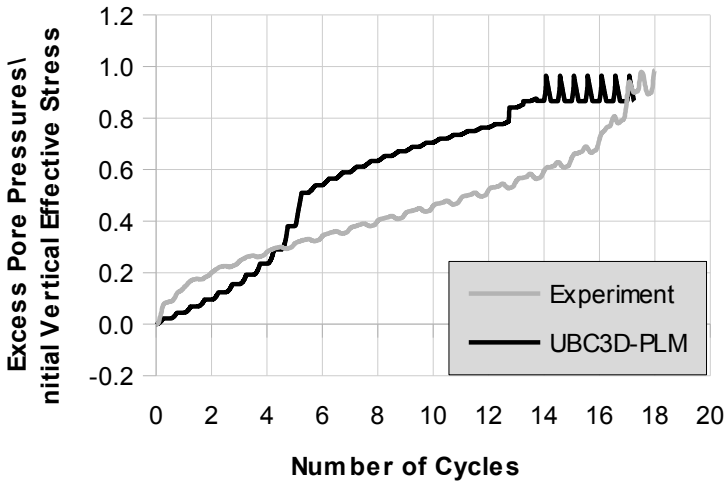

Figure 2.8: Validation of the UBC3D-PLM for cyclic loading. Evolution of the excess pore pressure in Test 1. Influence of K_0. Fraser sand with $RD = 40\%$. $CSR = 0.12$. $K_0 = 0.5$.

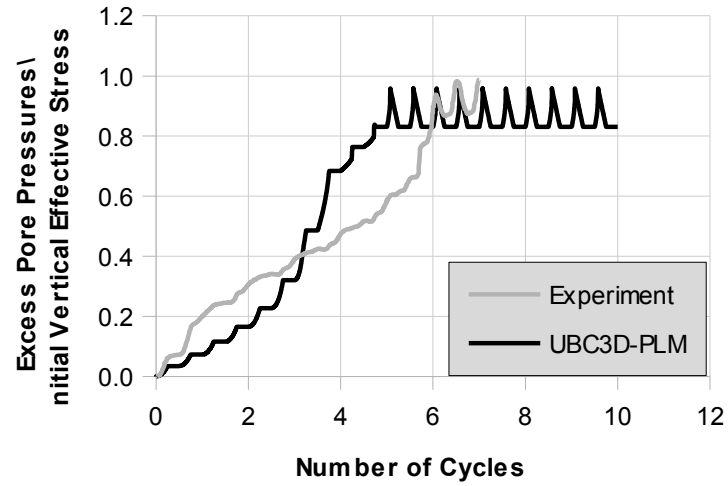

Figure 2.9: Validation of the UBC3D-PLM for cyclic loading. Evolution of the excess pore pressure in Test 2. Influence of K_0. Fraser sand with $RD = 40\%$. $CSR = 0.1$. $K_0 = 0.5$.

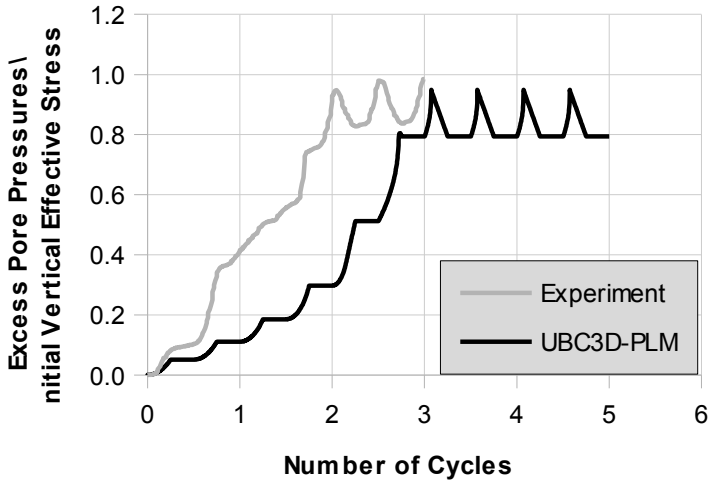

Figure 2.10: Validation of the UBC3D-PLM for cyclic loading. Undrained behaviour of Fraser sand ($RD = 40\%$) under cyclic simple shear. Influence of K_0. Stress path in Test 3 with $CSR = 0.12$. $K_0 = 0.5$.

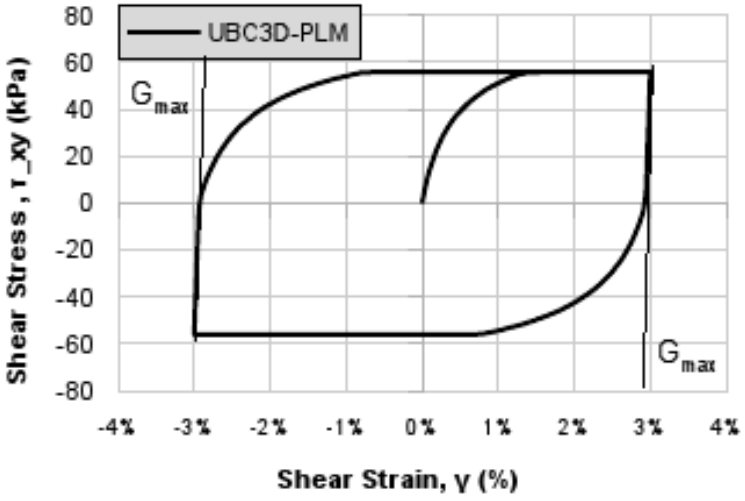

Figure 2.11: Over-produce of hysteretic damping of the UBC3D-PLM constitutive model. The elastic unloading with G_{max} leads to over-produced damping.

Chapter 3

Validation of the UBC3D-PLM in a finite element scheme

3.1 Modelling of a dynamic centrifuge

In this chapter the validation of the UBC3D-PLM in a finite element scheme using PLAXIS 2D is presented. A dynamic centrifuge is modelled. The parameters for the numerical model as well as the experimental results for the comparison are reported by Byrne et al. (2004).

The main objective in this numerical calculation is to test the ability of the proposed model to capture the onset of liquefaction and judge the accuracy of the results in terms of the evolution of excess pore pressures during dynamic loading. The predicted soil behaviour is compared with measurements taken during the physical modelling.

A systematization of the centrifuge test is presented in Figure 3.1. The magnitude of the acceleration applied to the centrifuge equals 120 g (g is the gravitational acceleration) in order to scale the stresses during the physical modelling. The input motion for the dynamic loading is 50 cycles of applied

acceleration equals 0.2 g and the frequency equals 1.5 Hz. The depth of the soil after the scaling factor is presented Figure 3.1. Based on this depth the numerical model is developed.

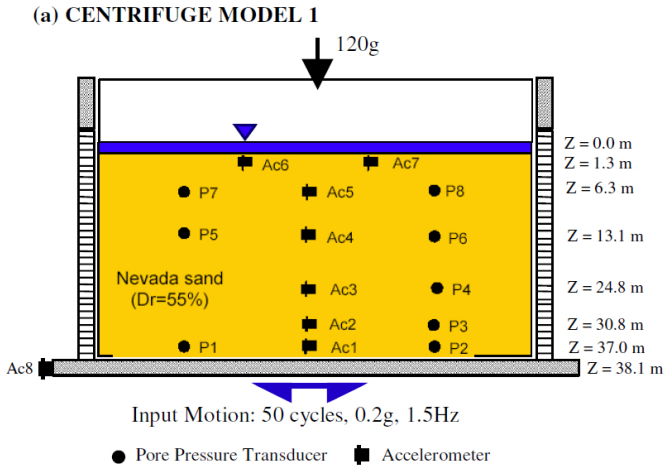

Figure 3.1: Numerical modelling of a dynamic centrifuge and comparison with the results of the physical modelling (Byrne et al., 2004).

Figure 3.2 presents the finite element mesh which is used in the numerical calculation for the plane-strain model. A regular mesh with 660 elements (15-nodes per element) is chosen. In dynamic calculations the regular fine mesh gives the highest accuracy in the reproduced numerical results. A rigid base is used as the horizontal boundary at the bottom with prescribed horizontal displacement in order to enter the dynamic load in the model.

The nodes on the right vertical boundary are in the exact same height as the nodes in the left vertical boundary and are tied together. With this procedure the displacements modes of the rings which are used in the physical model can be numerically represented (Byrne et al., 2004). The input acceleration imported in PLAXIS 2D for the purpose of the dynamic phase of the calculation and is shown in Figure 3.3. The total time of the input acceleration is 33 sec. The input signal determined every 0.01 sec.

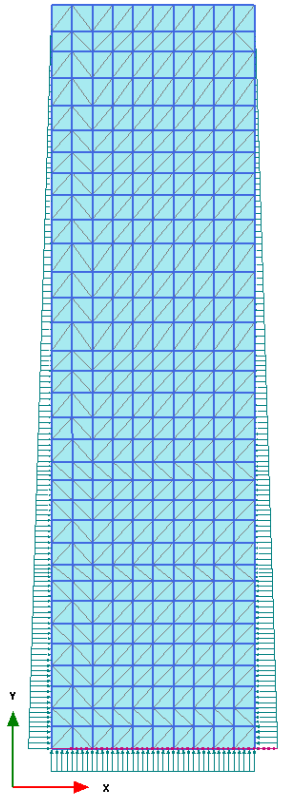

Figure 3.2: The finite element mesh used for the numerical modelling of the dynamic centrifuge in PLAXIS 2D. 660 elements. 15-nodes per element.

Finally, 3300 dynamic steps are chosen for the calculation and 1 dynamic sub-step in every step.

The soil which is tested in the centrifuge test is a medium dense Nevada sand with relative density 55%. No element tests are published for the specific soil used in the centrifuge. The parameters for the numerical model are initially extracted using the generic equations for calibration of UBCSAND published by Beaty and Byrne (2011) and slightly modified after calibration with published experimental data of Nevada sand (Kammerer et al., 2004).

The generic calibration equations proposed by Beaty and Byrne (2011)

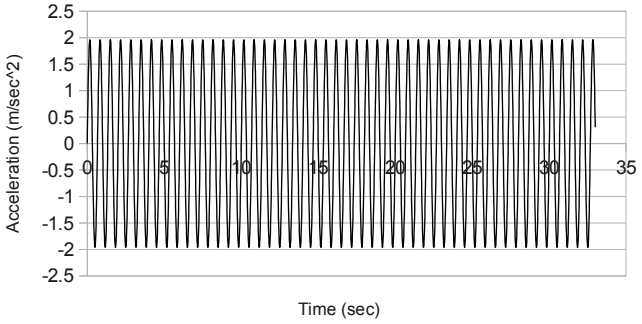

Figure 3.3: Total dynamic loading time 33 seconds. 50 loading cycles. The amplitude of acceleration equals 1.96 m/s^2. The frequency equalas 1.5 Hz.

are extracted after calibration of UBCSAND with experimental data. The use of them in UBC3D-PLM should always be followed from a verification process with specific experimental results. The parameters are summarized in Table 3.1. The consolidation phase is calculated with a K_0 procedure in PLAXIS. The K_0 assumed 0.5 for this case.

$\phi_p(^\circ)$	$\phi_c(^\circ)$	K_B^e	K_G^e	K_G^p	$me = ne$	np	R_f	$N1_{60}$	fac_{hard}
34	31	721	1031	700	0.5	0.4	0.74	10	0.7

Table 3.1: **Input parameters for modelling the dynamic centrifuge. The post post liquefaction factor fac_{post} equals 0.6.**

3.2 Results and discussion

Figure 3.4 presents the predicted acceleration during the test both in the physical and in the numerical model. The numerical results are adequately accurate at a lower depth but the residual acceleration which is mobilized in the soil in the deeper layers does not represent the real soil behaviour observed in the physical model. During this project the influence of the elasticity parameters on the propagation of the shear waves has also been

checked but the results are not further improved. The residual acceleration in the soil is most likely due to rigid base used for the modelling.

Figure 3.5 presents the predicted accumulation of the excess pore pressure and the comparison with the experimental result. At 13.1 meters depth the numerical prediction shows a very good agreement with the results from the physical model. It can be seen that initially in the experiment the dynamic loading starts a bit later from the numerical calculation but the slopes of both curves are almost identical. That means that the behaviour of the constitutive model is very accurate for this case. The maximum effective stress mobilized during consolidation in the experiment is higher than the prediction, however, a small deviation in the input parameters for this soil is highly likely. It can be concluded that the UBC3D-PLM can predict the onset of liquefaction with adequate accuracy for this depth.

At 24.8 meters depth the onset of liquefaction is again predicted with adequate accuracy, however, the model predicts a much more rapid evolution of the excess pore pressure than the observed evolution during the experiment. The evolution of the excess pore pressure becomes slower after the first cycles and finally the onset of liquefaction is predicted in approximately 10 seconds which is a very good representation of the behaviour observed in the experiment. The maximum vertical effective stress which is predicted by PLAXIS during consolidation is slightly lower also for this depth.

At 30.8 meters depth the onset of liquefaction is predicted in 10 seconds which also represents the observed soil behaviour. However, the inaccuracy in the evolution of the excess pore pressure becomes higher for higher depth. The accumulation of excess pore pressures is overestimated in the initial cycles by the UBC3D-PLM. The final accumulated excess pore pressures are also overestimated by PLAXIS but the onset of liquefaction is again predicted with adequate accuracy for this case.

It is concluded by the comparison of the experimental with the numerical results that the stress densification rule plays a significant role. This leads

to an initial rapid evolution of the excess pore pressures in deeper depths. The effect of the confining pressure in the cyclic resistance of the soil has to be included in a future reformulation. It can finally be seen that the residual acceleration after the first 10 seconds influences more the post-liquefaction soil behaviour.

Figure 3.6 presents the stress path in $p' - q$ stress space reproduced for a stress point at 13.1 m depth. The stress path does not start from the isotropic axis as expected. At Point (a) the accumulated stress path touches the peak stress level defined by the input peak friction angle. The secondary yield surface is deactivated and the primary yield surface is solely used for the rest of the test. The densification rule is finally not activated. At Point (b) dilation is predicted by the model and negative excess pore pressures (compression) are generated during the test. This process slows down the evolution of the excess pore pressures during dynamic loading.

Figure 3.7 presents the stress path in a $p' - q$ stress space for a stress point at 24.8 m depth. Primary loading initially occurs at Point a and this causes a rapid evolution of the excess pore pressure which is presented before. The plastic shear modulus during primary loading is not influenced by the effective confining pressure in this high depth, due to the limitation in the UBC3D-PLM formulation. After a full cycle that the stiffness of the primary yield surface is used, for half a cycle the densification rule is used till the stress path touches the peak stress level at Point (b). After that the secondary yield surface is deactivated and the primary yield surface is used till the end of the test.

Figure 3.8 presents the stress path in $p' - q$ stress space for a stress point at 30.8 m depth. At Point (a) the primary yield surface is used which predicts a very rapid evolution of excess pore pressure caused by the absence of the stress densification rule. At Point (b) the densification rule is activated during the expansion of the secondary yield surface. This slows down the evolution of the pore pressures. At Point (c) the primary yield surface is

used again when the stress path exceeds the previous maximum mobilized stress state. At Point (d) the densification rule is activated again and it is the mechanism that slows down finally the evolution of the excess pore pressure which leads to adequate accuracy in the liquefaction prediction. At Point (e) the secondary yield surface is deactivated because the stress path reached the peak stress state.

It can be concluded from the investigation of the stress paths that the absence of a stress densification rule leads to rapid evolution of the excess pore pressure in higher depths during the first loading cycles. UBC3D-PLM does not include the influence of the effective confining pressure on the cyclic resistance of the soil. Moreover, the soil densification rule which is implemented during this research helps for a better prediction of the onset of liquefaction, however, it works consistently only in the case of symmetric loading and for stress path starts from the isotropic axis. A more advanced framework for the function of both the yield surfaces is recommended for future research.

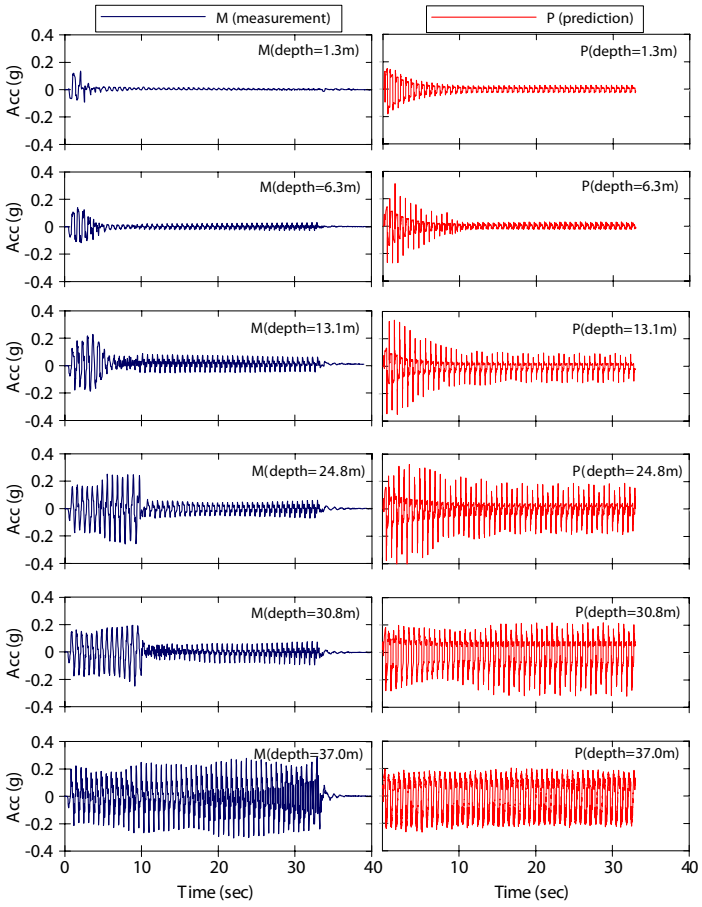

Figure 3.4: Comparison of the predicted acceleration in different depths during the dynamic loading with the experimental results. Measurements from the physical model and predictions from PLAXIS.

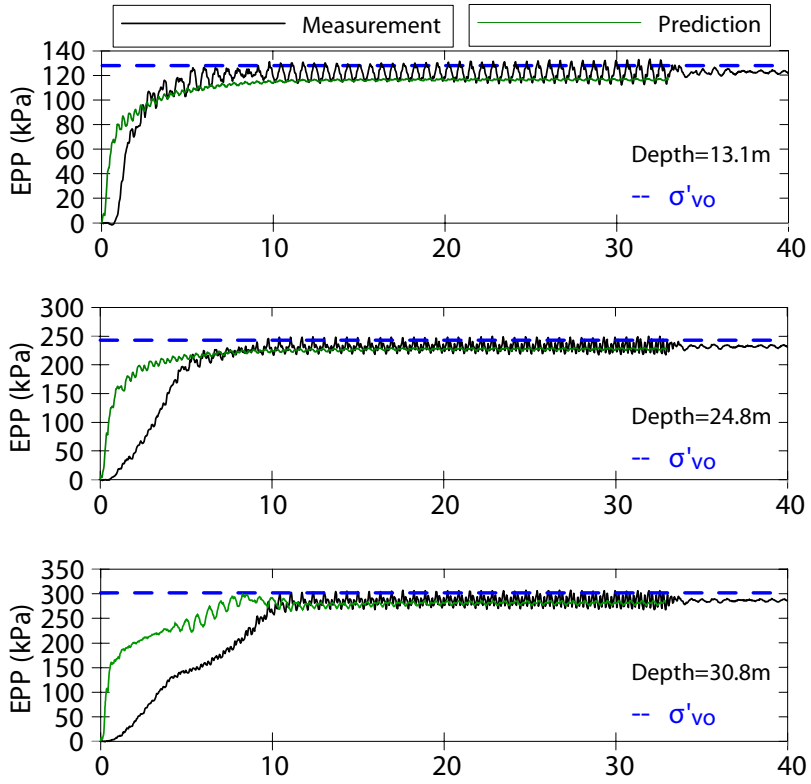

Figure 3.5: Comparison of the predicted evolution of excess pore pressure by the modified UBC3D-PLM with the experimental results of a dynamic centrifuge. Measurements from the physical model and predictions from PLAXIS.

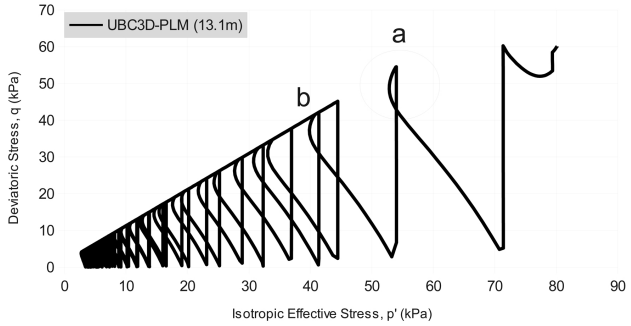

Figure 3.6: Comparison of the predicted evolution of excess pore pressure by the modified UBC3D-PLM with the experimental results of a dynamic centrifuge. Point a: Deactivation of the secondary yield surface. Point b: Dilatancy prediction.

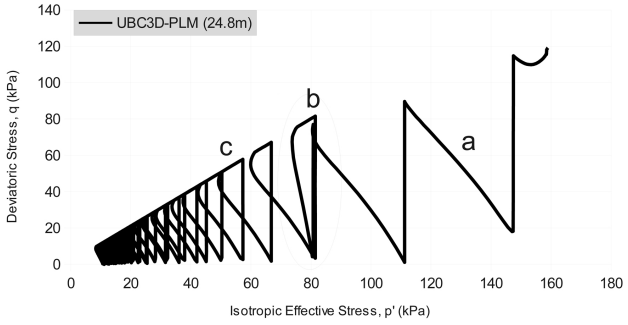

Figure 3.7: Reproduced stress path in a $p' - q$ stress space during the numerical modelling of the dynamic centrifuge. Stress point at 24.8 m depth. Point a: Primary yield surface is used. Point b: Deactivation of the secondary yield surface.

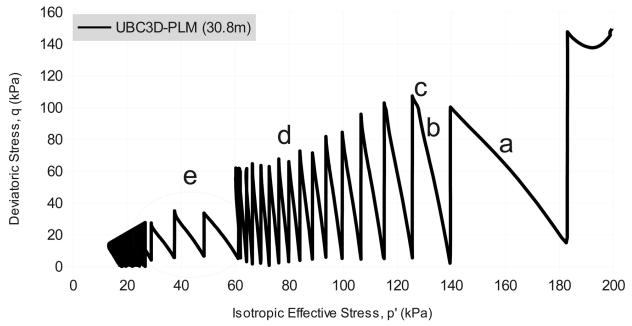

Figure 3.8: Reproduced stress path in a $p' - q$ stress space during the numerical modelling of the dynamic centrifuge. Stress point at 30.8 m depth. Point a: The primary yield surface is used. Point b: Densification rule. Point c: The primary yield surface is used. Point d: Soil densification. Point e: Deactivation of the secondary yield surface.

Bibliography

M. Beaty and P. Byrne. An effective stress model for predicting liquefaction behaviour of sand. *Geotechnical Earthquake Engineering and Soil Dynamics III ASCE Geotechnical Special Publication No.75*, 1:766–777, 1998.

M.H. Beaty and P.M. Byrne. Ubcsand constitutive model version 904ar. *Itasca UDM Web Site*, page 69, 2011.

P. M. Byrne, S. S. Park, M. Beaty, M. Sharp, L. Gonzales, and T. Abdoun. Numerical modelling of dynamic centrifuge tests. *13^{th} World Conference in Earthquake Engineering*, 2004.

A. M. Kammerer, J. Wu, J. M. Pestana, M. Riemer, and R. B. Seed. Cyclic simple shear testing of nevada sand for peer center project 2051999. *University of California, Berkley*, Geotechnical Engineering Report No. UCB/GT/00-01, 2004.

G.R. Martin, W.D.L. Finn, and H.B. Seed. Fundamentals of liquefaction under cyclic loading. *Journal of the Geotechnical Engineering Division, ASCE*, 101, 1975.

E. Naesgaard. A hybrid effective stress-total stress procedure for analysing soil embankments subjected to potential liquefaction and flow. *PHD Thesis in the University of British Columbia*, 2011.

S.S. Park and P.M. Byrne. Practical constitutive model for soil liquefaction. *Intl. Conf. on Cyclic behaviour of soils and liquefaction*, pages 571–580, 2004.

D.M. Potts and L. Zdravkovic. Finite element analysis in geotechnical engineering. theory. *Thomas Telford Publishing*, 1999.

H. Puebla, M. Byrne, and P. Phillips. Analysis of canlex liquefaction embankments prototype and centrifuge models. *Canadian Geotechnical Journal*, 34:641–657, 1997.

P. W. Rowe. The stress-dilatancy relation for static equilibrium of an assembly of particles in contact. *Proc. R. Soc.*, 269A:500–527, 1962.

S. Sriskandakumar. Cyclic loading response of fraser sand for validation of numerical models simulating centrifuge tests. *Master's thesis, The University of British Columbia, Department of Civil Engineering*, 2004.

A. Tsegaye. Plaxis liqueafaction model. report no. 1. *PLAXIS knowledge base.*, 2010.

Y.P. Vaid, M. Uthayakumar, S. Sivathayalan, P.K. Robertson, and B. Hofmann. Laboratory testing of syncrude sand. *48th Candian Geotechnical Conference, Vancouver, B.C.*, 1:223–232, 1995.